Design and Optimization of CPW Circuits Using EM-ANN Models for CPW Components

Paul M. Watson and Kuldip C. Gupta, *Fellow, IEEE*

***Abstract*— Accurate and efficient electromagnetically trained artificial neural-network (EM-ANN) models have been developed for coplanar waveguide (CPW) circuit components. Modeled components include: CPW transmission lines (frequency dependent Z_o and ε_{re}), 90° bends, short-circuit stubs, open-circuit stubs, step-in-width discontinuities, and symmetric T-junctions. These models allow for circuit design, simulation, and optimization within a commercial microwave circuit simulator environment, while providing the accuracy of electromagnetic (EM) simulation. Design and optimization of a CPW folded double-stub filter and a 50-Ω 3-dB power divider circuit using the developed CPW EM-ANN models are demonstrated.**

***Index Terms*— CAD, CPW circuits, CPW models, neural networks.**

I. Introduction

COPLANAR waveguide (CPW) circuits offer several advantages due to the CPW configuration, such as the ease of shunt and series connections, low radiation, low dispersion, and avoidance of the need for thin fragile substrates. These advantages make CPW an attractive choice for development of monolithic microwave integrated circuits (MMIC's). Currently, design software available for CPW circuits is inadequate because of the nonavailability of accurate and efficient models for CPW discontinuities such as bends, T-junctions, steps-in-width, short and open stubs, etc. Accurate characterization and modeling of these components are vital for accurate circuit simulation and increased first-pass design success.

Much effort has been expended in developing accurate and efficient methods for electromagnetic (EM) simulation of CPW discontinuities [1]–[33]. However, the time-consuming nature of EM simulation limits the use of these tools for interactive CAD and circuit optimization. Equivalent circuit models generally available for CPW discontinuities require certain assumptions to be made which may or may not be valid over the desired range of operation. CPW discontinuities have also been characterized by measurements [34], [35], generating a library of data which is generally valid only for the structures measured. This method of characterization is also very time consuming.

As an alternative to the above, we have developed electromagnetically trained artificial neural-network (EM-ANN) models for CPW components suitable for use in interactive MMIC design and optimization. No assumptions about component behavior are made when developing the EM-ANN models. Full-wave EM simulation has been employed to characterize the CPW components. EM-ANN models have been developed for CPW transmission lines (frequency dependent Z_o and ε_{re}), 90° bends, short-circuit stubs, open-circuit stubs, step-in-width discontinuities, and symmetric T-junctions. Air-bridges are included where needed to suppress the unwanted slot-line mode [36]. All models have been developed using HP-Momentum[1] for EM simulation and its adaptive frequency-sampling (AFS) feature, with the exception of the CPW transmission-line model. This was due to the unavailability of Z_o information for CPW lines in HP-Momentum. Common parameters for all models are the substrate parameters ($\varepsilon_r = 12.9$, $H_{sub} = 625$ μm, $\tan\delta = 0.0005$) and air-bridge parameters ($H_a = 3$ μm and $W_a = 40$ μm). Once developed, these EM-ANN models are linked to a commercial microwave-circuit simulator where they provide accuracy approaching that of the EM-simulation tool used for characterization of the CPW components over the entire ranges of the model input variables. In addition, the developed models allow for very fast and accurate EM/circuit optimization within the framework of the circuit-simulator environment.

Circuit design using the developed EM-ANN CPW models is demonstrated by two examples: a CPW folded double-stub filter and a 50-Ω 3-dB power-divider circuit. Optimization of circuit responses have been performed and compared to the full-wave simulation results of the entire circuits, showing excellent agreement.

II. EM-ANN Modeling

The methodology used for developing accurate and efficient EM-ANN models has been discussed and demonstrated in [37] and [38]. Briefly, the ANN architecture used in this paper is shown in Fig. 1 and consists of an input layer, an output layer, and one hidden layer. It is a multilayer feed-forward ANN, utilizing the error-backpropagation learning algorithm [39]. The hidden layer, which incorporates nonlinear

Manuscript received March 31, 1997; revised August 15, 1997.

The authors are with the Center for Advanced Manufacturing and Packaging of Microwave, Optical, and Digital Electronics (CAMPmode) and the Department of Electrical and Computer Engineering, University of Colorado, Boulder, CO 80309-0425 USA.

Publisher Item Identifier S 0018-9480(97)08350-6.

[1] HP-Momentum, version A.02.00, Hewlett-Packard Company, Santa Rosa, CA, 1995.

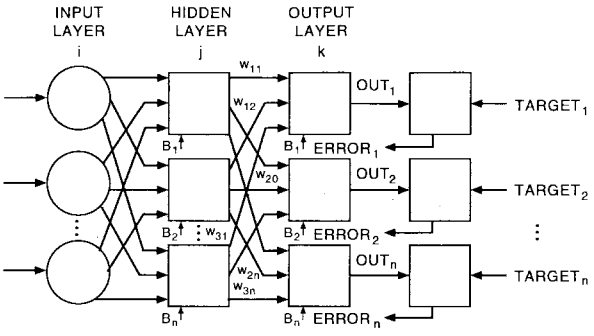

Fig. 1. Artificial neural-network architecture.

activation functions, allows modeling of complex input/output relationships between multiple inputs and multiple outputs. Inputs are connected to the hidden layer by one set of weights and the hidden layer is connected to the output layer by another set of weights. Training of the EM-ANN model is accomplished by adjusting these weights to give the desired response.

The ANN learns relationships among sets of input/output data (referred to as "examples" throughout the remainder of this paper) which are characteristic of the component under consideration. First, the input vectors of the training dataset are presented to the input neurons and output vectors are computed. ANN outputs are then compared to the known outputs (of the training dataset) and errors are computed. Error derivatives are then calculated and summed up for each weight until all the training examples have been presented to the network. These error derivatives are then used to update the weights for neurons in the model. Training proceeds until errors are lower than prescribed values. Details of the training algorithm are given in [40].

In order to train the EM-ANN models, a number of EM simulations need to be performed. These simulation points need to be chosen so that important input/output relationships are presented to and learned by the EM-ANN model. Simple models require less simulation points, while highly nonlinear models require an increased number of simulations. Structures for EM simulation are chosen using design of experiments (DOE) methodology [41]. Although DOE methods had been developed for regression analysis, they can be used to determine simulation points which effectively cover the region of interest. When building a model, one would like to perform as few EM simulations as possible for achieving the desired accuracy. This requires starting with a low-order experimental design and sequentially building up to higher order designs by adding additional simulation points.

III. EM-ANN Modeling of Chamfered CPW 90° Bends

In this section, EM-ANN models are developed for two different chamfered CPW bend structures [42], as shown in Fig. 2. Air-bridges are placed near CPW bends in order to reduce the unwanted slot-line mode which tends to radiate [36]. The slot-line mode is generated in CPW bends due to the path-length difference of the slots. However, the inclusion

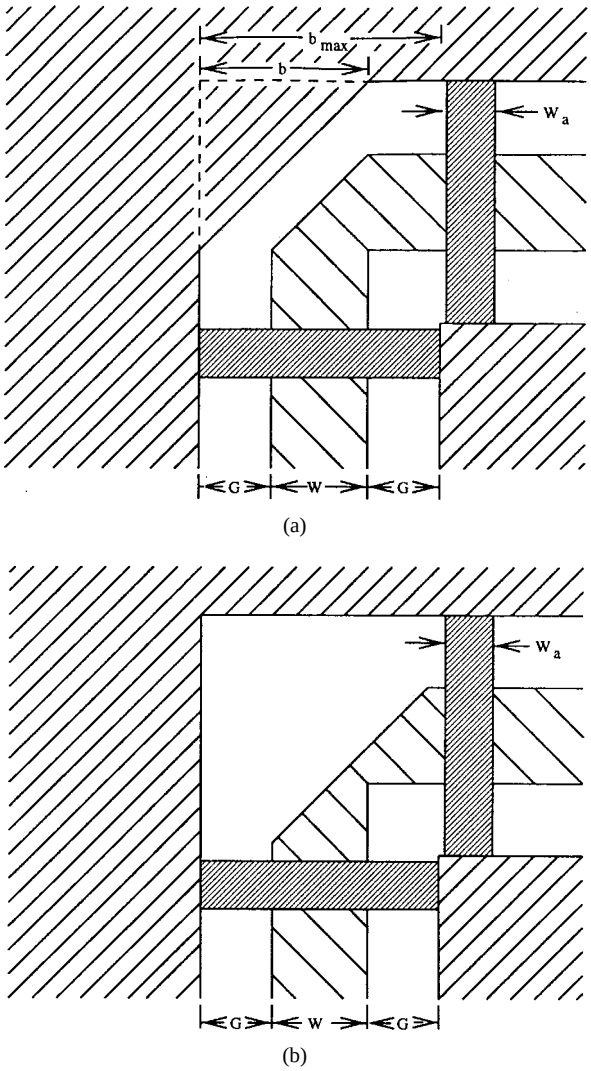

Fig. 2. CPW 90° bend structures with $W_a = 40\ \mu$m, $H_a = 3\ \mu$m, $H_{\rm sub} = 625\ \mu$m, $\varepsilon_r = 12.9$, and $\tan\delta = 0.0005$. (a) Conventional chamfered bend and (b) novel compensated bend (H_a is height of air-bridge above the substrate and $H_{\rm sub}$ is the substrate thickness).

of air-bridges adds unwanted capacitance which can degrade the performance of the bend. In addition to compensating for the reactances associated with the bend, chamfering provides a simple way to partially compensate for the effects of the air-bridges. We investigate the effects of chamfering on the S-parameters for the CPW 90° bends shown in Fig. 2. Optimal chamfering values are determined for the different bend structures.

CPW bends of the type shown in Fig. 2(a) have been studied in [3], but only for $b = 0$ and $b = W + G$. The work reported in [3] is extended by determining the optimal chamfer for each bend structure. The compensated CPW bend [shown in Fig. 2(b)] is a novel structure which has been shown by EM simulation to improve upon the return loss and the insertion loss of the conventional chamfered bend of Fig. 2(a). EM-ANN models are developed for the CPW bends and are used to determine optimal chamfer values. All air-bridge parameters are held constant in order to concentrate on the effects caused by the chamfering of the bends.

TABLE I
VARIABLE PARAMETER RANGES FOR CPW COMPONENTS

	Min.	Max.
Frequency	1 GHz	50 GHz
W	20 μm	120 μm
G	20 μm	60 μm

TABLE II
ERROR RESULTS (AVERAGE AND STANDARD DEVIATION) BETWEEN THE EM-ANN MODEL AND FULL-WAVE SIMULATION FOR THE OPTIMALLY CHAMFERED CPW BEND

	$\lvert S_{11}\rvert$	$\angle S_{11}(°)$	$\lvert S_{21}\rvert$	$\angle S_{21}(°)$
Train/test dataset				
Average error	0.000701	0.102	0.000293	0.034
Standard dev.	0.000632	0.104	0.000270	0.029
Verification dataset				
Average error	0.000966	0.124	0.000354	0.048
Standard dev.	0.001058	0.141	0.000339	0.039

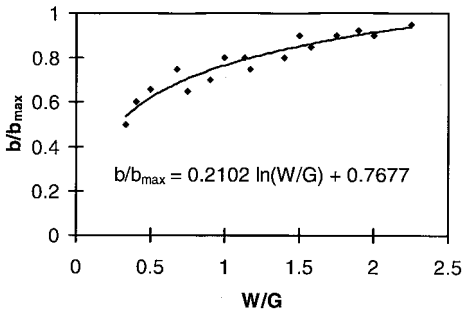

Fig. 3. Optimal chamfer for return loss versus W/G for the conventional bend of Fig. 2(a).

A. Optimally Chamfered Conventional CPW Bend

An EM-ANN model has been developed for the CPW bend structure shown in Fig. 2(a). Variable inputs for the EM-ANN model are W, G, $b/b_{\max}$, and frequency. Model outputs are S-parameters. Substrate material used is GaAs ($\varepsilon_r = 12.9$), and the thickness is 625 μm for all results included in this paper. Air-bridges are 40 μm wide (W_a), 3 μm (H_a) above the GaAs surface, and are positioned at the bend discontinuity as shown. Note, all air-bridge parameters are held constant in order to concentrate on the effects caused by the chamfering of the bends.

EM simulations were performed on 17 bend structures, included within the range of parameters given in Table I. Characteristic impedances used for port terminations have been determined from linecalc.[2] Five different values of chamfer were simulated for each bend, with $b/b_{\max}$ ranging from 0 to 1. The strip corner was chamfered by a proportional amount given by $bW/(W+G)$. EM simulation data was separated into training/test (165 examples) and verification (300 examples) datasets for model development. Ten neurons were used in the hidden layer. Error results (EM-ANN model compared to EM simulation) are shown in Table II.

It was determined that indeed there exists an optimal chamfer for each structure, especially when analyzing the return loss $20\log_{10}|S_{11}|$. The developed EM-ANN model can reproduce the trends in S-parameters determined by the changes in the physical structure of the CPW bend. Using this model, the optimal chamfer for each bend is determined. Fig. 3 shows the optimal chamfer $b/b_{\max}$ versus W/G for minimum return loss, as determined by the EM-ANN model. The optimal chamfer as a function of W/G is given by

$$\begin{aligned} b/b_{\max} &= 0.2102\ln(W/G) + 0.7677, && \text{for } 0 \le W/G \le 2 \\ &= 1, && \text{for } W/G > 2.5. \end{aligned} \tag{1}$$

[2] linecalc, version 5.0, Hewlett-Packard Company, Santa Rosa, CA, 1994.

TABLE III
ERROR RESULTS (AVERAGE AND STANDARD DEVIATION) BETWEEN THE EM-ANN MODEL AND FULL-WAVE SIMULATION FOR THE COMPENSATED BEND

	$\lvert S_{11}\rvert$	$\angle S_{11}(°)$	$\lvert S_{21}\rvert$	$\angle S_{21}(°)$
Train/test dataset				
Average error	0.000784	0.680	0.000584	0.363
Standard dev.	0.000518	0.513	0.000390	0.261
Verification dataset				
Average error	0.001390	1.022	0.000705	0.447
Standard dev.	0.000861	0.759	0.000365	0.380

TABLE IV
COMPARISON OF RETURN LOSS FOR THE CONVENTIONAL OPTIMALLY CHAMFERED BEND AND THE NOVEL COMPENSATED BEND FOR SEVERAL STRUCTURES. (FREQUENCY = 50 GHz)

W (μm)	G (μm)	Optimally Chamfered bend Return loss (dB)	Novel bend Return loss (dB)	Improvement (dB)
70	60	-13.89	-20.92	7.03
120	40	-12.96	-16.36	3.40
70	20	-21.51	-26.94	5.43
35	55	-17.27	-20.18	2.91
105	55	-12.50	-17.02	4.52
105	25	-15.76	-19.33	3.57
70	40	-16.36	-21.41	5.05

B. Novel Compensated CPW Bend

An EM-ANN model has been developed for the novel compensated CPW bend structure proposed here and shown in Fig. 2(b). This novel bend is capable of improving upon the performance of the already discussed optimally chamfered CPW bend. Variable input parameters for the model are W, G, and frequency. Model outputs are S-parameters. For this novel bend, the optimum chamfer for the strip is found to be the maximum allowable by air-bridge placement. EM simulations have been performed on 17 bend structures, included within the range of parameters given in Table I, to provide training/test (45 examples) and verification (35 examples) datasets for model development. Ten neurons were used in the hidden layer. Error results for the developed EM-ANN model are shown in Table III.

C. CPW Bend Comparisons

The novel compensated CPW bend structure is found to improve the return loss over the optimally chamfered conventional bend, as shown in Table IV. We believe this to be due to a decrease in capacitance as the slot width at the

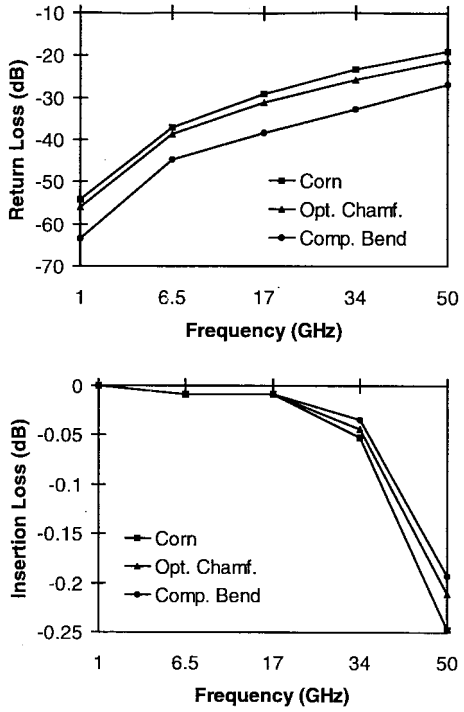

Fig. 4. Comparison of unchamfered (Corn), conventional (Opt. Chamf.), and novel (Comp. Bend) CPW bends. $W = 70\ \mu$m and $G = 20\ \mu$m.

corner is increased, thereby compensating for the increase in capacitance due to the air-bridges. Improvements are also seen in the insertion loss. Note that all air-bridge parameters remain the same as in the case for the optimally chamfered CPW bend.

Comparisons between unchamfered CPW corner, optimally chamfered conventional bend, and the novel compensated bends are shown in Fig. 4 for CPW bend structures with $W = 70\ \mu$m and $G = 20\ \mu$m, corresponding to $Z_o = 35\ \Omega$. Note that all air-bridges and reference planes are at the same positions. Based on the results shown in Fig. 4 and in Table IV, we note that the new compensated bend provides significant improvements in return and insertion loss over the other CPW bend structures. Improvements are also seen when comparing the optimally chamfered bend results to the corner (unchamfered) bend.

IV. EM-ANN Modeling of CPW Transmission Lines

An EM-ANN model has been developed for frequency dependent CPW transmission lines. Variable input parameters and corresponding ranges are given in Table I. Model outputs are frequency dependent Z_o and $\varepsilon_{\rm re}$. The EM-ANN model has been trained using PCAAMT,[3] a program which provides full-wave solutions for printed transmission lines and general multilayer geometries.[4] The training/test dataset consisted of 265 examples, while the verification dataset contained 51 examples. Twenty neurons were used in the hidden layer. Error results between the developed EM-ANN model and the full-wave solution for the training/test and verification datasets are shown in Table V.

[3]HP-Momentum, version A.02.20, could not be used for this purpose because the value of Z_o is not available for CPW.

[4]PCAAMT, version 2.0, EM-CAD Laboratory, Polytechnic University of New York, Brooklyn, NY, 1990.

TABLE V
Error Results (Average and Standard Deviation) Between the EM-ANN Model and Full-Wave Simulation for the CPW Transmission Line

	Z_o (Ω)	Z_o (%)	ε_{re}
Train/test dataset			
Average error	0.105	0.234	0.00283
Standard dev.	0.098	0.224	0.00248
Verification dataset			
Average error	0.111	0.243	0.00341
Standard dev.	0.112	0.238	0.00240

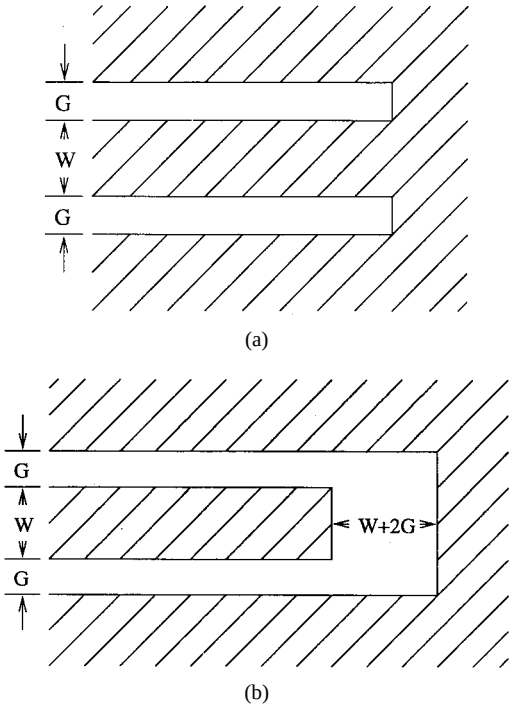

Fig. 5. CPW (a) short-circuit stub and (b) open-circuit stub geometries.

V. EM-ANN Models for CPW Open- and Short-Circuit Stubs

Open- and short-circuit stubs are important components for many circuit designs such as filters and impedance-matching networks. The geometries of the open- and short-circuit stubs considered are shown in Fig. 5. Variable input parameters and corresponding ranges for model development are given in Table I. Model outputs are S-parameters. Typical output responses for an open and a short circuit with reference planes at the discontinuities are shown in Fig. 6. For each model, EM simulations have been performed on 17 structures over the 1–50-GHz frequency range. For the short-circuit model development, 71 examples were used in the training/test dataset and 46 examples for the verification dataset, requiring five neurons in the hidden layer. Open-circuit model development was accomplished using 95 examples in the training/test dataset, 53 examples for the verification dataset, and six neurons in the hidden layer. Error results for the training and verification datasets are given in Table VI for the short circuit and in Table VII for the open circuit.

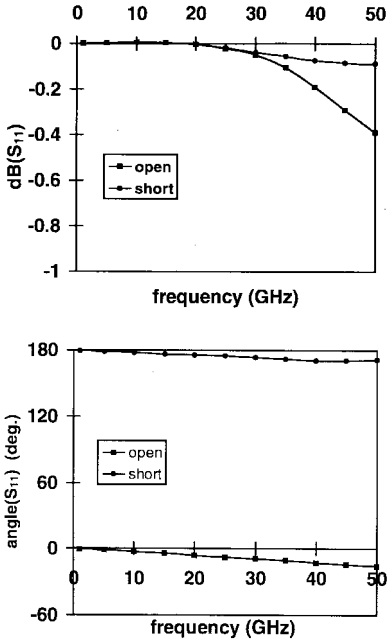

Fig. 6. S-parameter response for open and short-circuit stubs. $W = 70\ \mu$m, $G = 60\ \mu$m, and reference planes at the discontinuities.

TABLE VI
ERROR RESULTS (AVERAGE AND STANDARD DEVIATION) BETWEEN THE EM-ANN MODEL AND FULL-WAVE SIMULATION FOR THE CPW SHORT CIRCUIT OF FIG. 5(a)

	$\lvert S_{11}\rvert$	$\angle S_{11}$ (°)
Train/test dataset		
Average error	0.000248	0.396
Standard dev.	0.000350	0.271
Verification dataset		
Average error	0.000381	0.964
Standard dev.	0.000412	0.867

TABLE VII
ERROR RESULTS (AVERAGE AND STANDARD DEVIATION) BETWEEN THE EM-ANN MODEL AND FULL-WAVE SIMULATION FOR THE CPW OPEN CIRCUIT OF FIG. 5(b)

	$\lvert S_{11}\rvert$	$\angle S_{11}$ (°)
Train/test dataset		
Average error	0.000481	0.332
Standard dev.	0.000633	0.373
Verification dataset		
Average error	0.000520	0.634
Standard dev.	0.000892	0.676

VI. EM-ANN MODELING OF CPW STEP-IN-WIDTH

CPW step-in-width discontinuities are used extensively in circuit design for introducing impedance changes. The geometry of the step-in-width, for which an EM-ANN model has been developed, is shown in Fig. 7. Variable input parameters are frequency, W_1, W_2, and G. Also, only structures where $W_1 < W_2$ were used for model development due to the nature of the step. Parameter ranges for W_1, W_2, and G are given in Table I. Model outputs are S-parameters. A typical output response is shown in Fig. 8. EM simulations have been performed on 30 structures over the 1–50-GHz frequency range, providing 95 training/test examples and 55 verification examples. Eight neurons were used in the hidden layer. Residual errors are shown in Table VIII and (as for other models developed) are negligible for design applications.

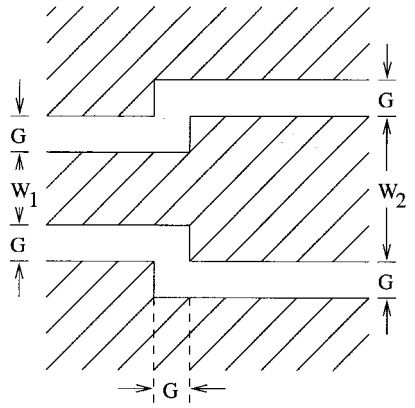

Fig. 7. CPW step-in-width geometry.

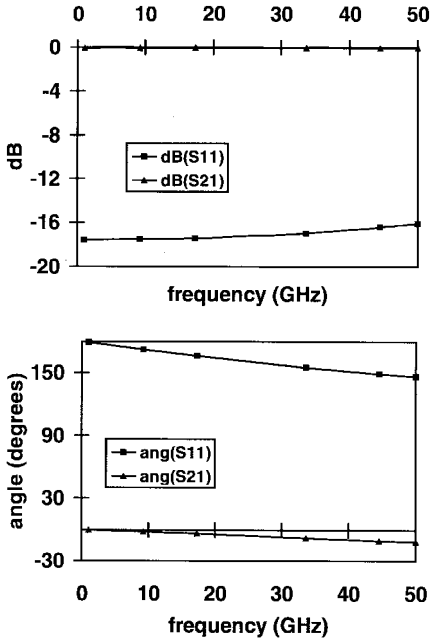

Fig. 8. S-parameter response for a 71–50-Ω CPW step-in-width transition. $W_1 = 20\ \mu$m, $W_2 = 70\ \mu$m, $G = 60\ \mu$m, and reference planes at the discontinuity.

TABLE VIII
ERROR RESULTS (AVERAGE AND STANDARD DEVIATION) BETWEEN THE EM-ANN MODEL AND FULL-WAVE SIMULATION FOR THE CPW STEP-IN-WIDTH

	$\lvert S_{11}\rvert$	$\angle S_{11}$(°)	$\lvert S_{21}\rvert$	$\angle S_{21}$(°)
Train/test dataset				
Average error	0.000864	0.435	0.000792	0.321
Standard dev.	0.000721	0.454	0.000840	0.286
Verification dataset				
Average error	0.001214	0.553	0.000986	0.457
Standard dev.	0.001023	0.579	0.001032	0.390

VII. EM-ANN MODELING OF CPW SYMMETRIC T-JUNCTIONS

The symmetric T-junction under consideration is shown in Fig. 9. Variable model input parameters are frequency, W_{in}, G_{in}, W_{out}, and G_{out}. Parameter ranges are given in Table I. Model outputs are S-parameters. A typical output response is shown in Fig. 10. EM simulations have been performed on 25

TABLE IX
ERROR RESULTS BETWEEN THE EM-ANN MODEL AND EM SIMULATION FOR THE CPW SYMMETRIC T-JUNCTION (AVERAGE AND STANDARD DEVIATION). INPUT BRANCHLINE PORT IS PORT 1 AND THE OUTPUT PORTS ON THE MAIN LINE ARE PORTS 2 AND 3

	$\lvert S_{11}\rvert$	$\angle S_{11}$ °	$\lvert S_{13}\rvert$	$\angle S_{13}$ °	$\lvert S_{23}\rvert$	$\angle S_{23}$ °	$\lvert S_{33}\rvert$	$\angle S_{33}$ °
Train								
Avg.	0.00150	0.754	0.00071	0.176	0.00084	0.246	0.00106	0.633
Stdev.	0.00128	0.696	0.00058	0.172	0.00097	0.237	0.00109	0.546
Verify								
Avg.	0.00345	0.782	0.00088	0.141	0.00126	0.177	0.00083	0.838
Stdev.	0.00337	0.674	0.00085	0.125	.00105	0.129	0.00068	0.717

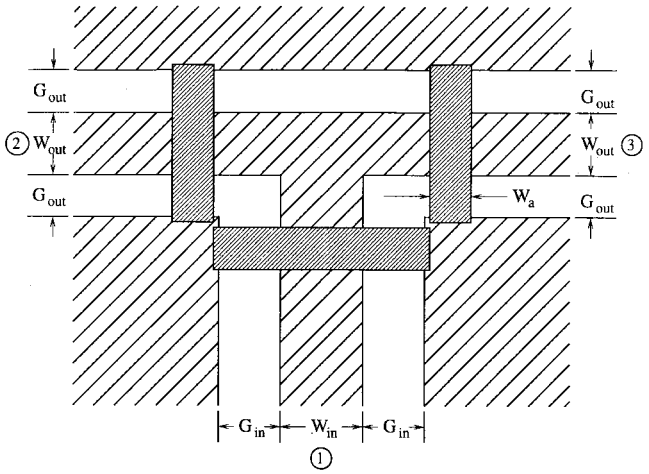

Fig. 9. CPW symmetric T-junction geometry.

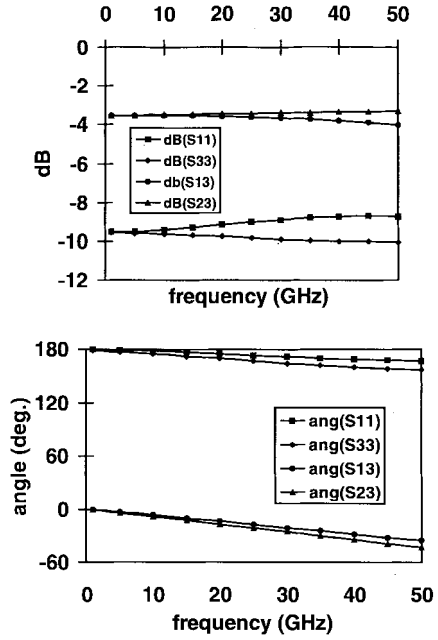

Fig. 10. S-parameter response for a typical CPW symmetric T-junction. $W_{\rm in} = W_{\rm out} = 70$ μm, $G_{\rm in} = G_{\rm out} = 60$ μm, and reference planes at the air-bridge locations.

structures over the 1–50-GHz frequency range, providing 155 training/test examples and 131 verification examples. Fifteen neurons were used in the hidden layer. Model error results are shown in Table IX for both the training/test and verification datasets.

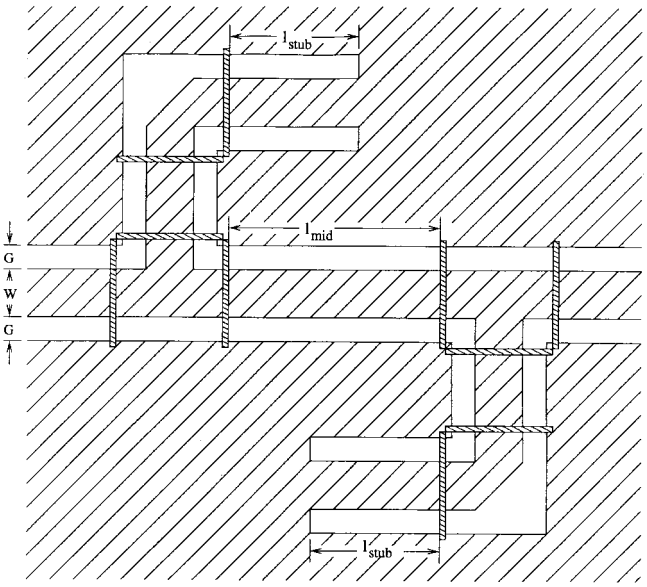

Fig. 11. CPW folded double-stub filter geometry.

VIII. CPW CIRCUIT-DESIGN EXAMPLES

A. CPW Folded Double-Stub Filter

The first CPW circuit-design example is a CPW folded double-stub filter, as shown in Fig. 11. For this design $W = 70$ μm and $G = 60$ μm, yielding $Z_o \approx 50$ Ω. CPW EM-ANN models used are CPW transmission line, 90° compensated bends, short-circuit stubs, and symmetric T-junctions. The filter has been designed for a center frequency of 26 GHz. Ideally, the length of each short-circuit stub and the section of line between the stubs should have a length of $\lambda/4$ at 26 GHz. However, due to the presence of discontinuities, these lengths need to be adjusted. Design and optimization have been accomplished using HP-MDS[5] network simulator and EM-ANN models for various components.

Parameters to be optimized are $l_{\rm stub}$ and $l_{\rm mid}$. Initial values for these lengths were determined and the structure simulated, showing a less than ideal response. The circuit was then optimized, using gradient descent, to provide the desired circuit response. The effect of optimization was a reduction in line lengths. Results are shown in Fig. 12 for the original design, optimized design, and full-wave EM simulation of the entire optimized circuit. Excellent agreement is obtained

[5]HP-MDS, version 6.02.00, Hewlett-Packard Company, Santa Rosa, CA, 1995.

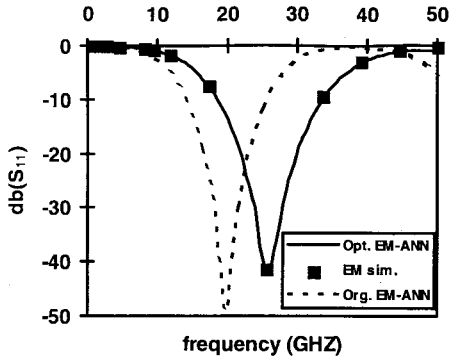

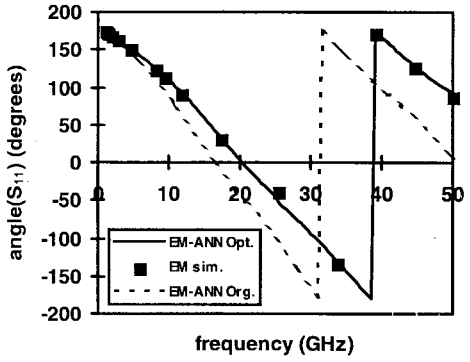

(a)

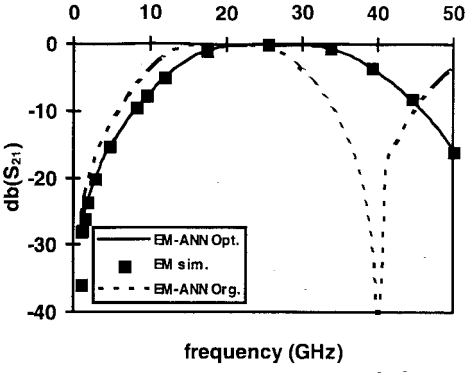

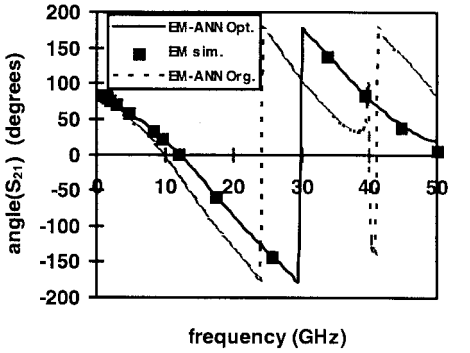

(b)

Fig. 12. CPW folded double-stub filter response for the optimized EM-ANN circuit (EM-ANN Opt.), the original EM-ANN circuit (EM-ANN Org.), and EM simulation (EM sim.). (a) S_{11} and (b) S_{21}.

between the optimized EM-ANN circuit design and the full-wave EM simulation over the 1–50-GHz frequency range. This

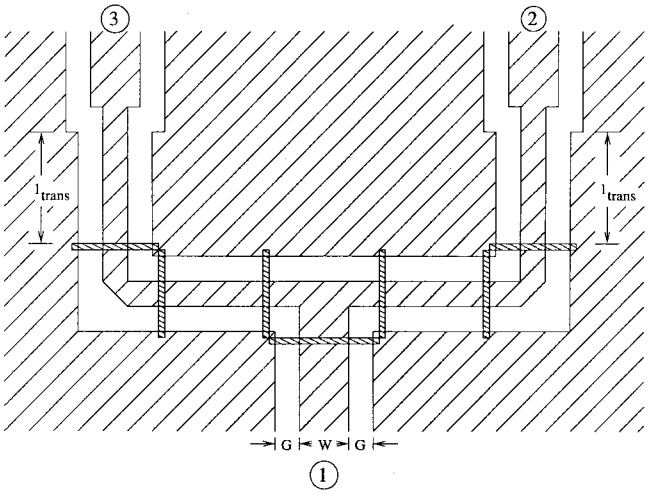

Fig. 13. CPW power-divider geometry.

demonstrates applications of EM-ANN models in CPW circuit design.

B. CPW 50-Ω 3-dB Power Divider

The second CPW circuit design example is a 50-Ω 3-dB power divider, shown in Fig. 13. For this design, EM-ANN models for CPW transmission lines, 90° compensated bends, T-junctions, and step-in-width transitions are used. The power divider has been designed for a 3-dB power split between the output ports at 26 GHz. Ideally, $\lambda/4$ 70.7-Ω line sections are used to transform the 50-Ω output impedance at Ports 2 and 3 into 100-Ω loads at the T-junction. Due to the presence of discontinuities, the lengths of the transformers need to be adjusted. Input and output lines are 50 Ω ($W = 70$ μm, $G = 60$ μm), and transformer lines are approximately 71 Ω ($W = 20$ μm, $G = 60$ μm). Again, HP-MDS[5] has been used for design and optimization.

The optimizable parameter for this design is the length of the transformer line section, $l_{\rm trans}$. An initial value for $l_{\rm trans}$ was determined. After the initial design failed to meet the prescribed design criteria, optimization was performed, resulting in a shorter line length than initially determined. Results are shown in Fig. 14 for the original design, optimized design, and full-wave EM simulation of the entire optimized circuit. As with the double-stub filter design, excellent agreement has been obtained between the optimized EM-ANN circuit design and EM-simulation results over the entire 1–50-GHz range.

Using EM-ANN models for CPW components has allowed accurate and efficient design and optimization of the CPW filter. In essence, the EM-ANN models provide EM optimization capabilities. Optimization time for the EM-ANN circuit was only 3 min and required seven circuit analyses. The amount of time required to provide EM simulation results for 17 frequency points for the entire filter circuit was approximately 14 h on an HP 700 workstation. Optimization time for the power divider circuit was only 2 min and required six circuit analyses. EM simulation time for the entire power divider, at 15 frequency points, totaled almost 11 h on an HP 700 workstation. This confirms that substantial savings in computer

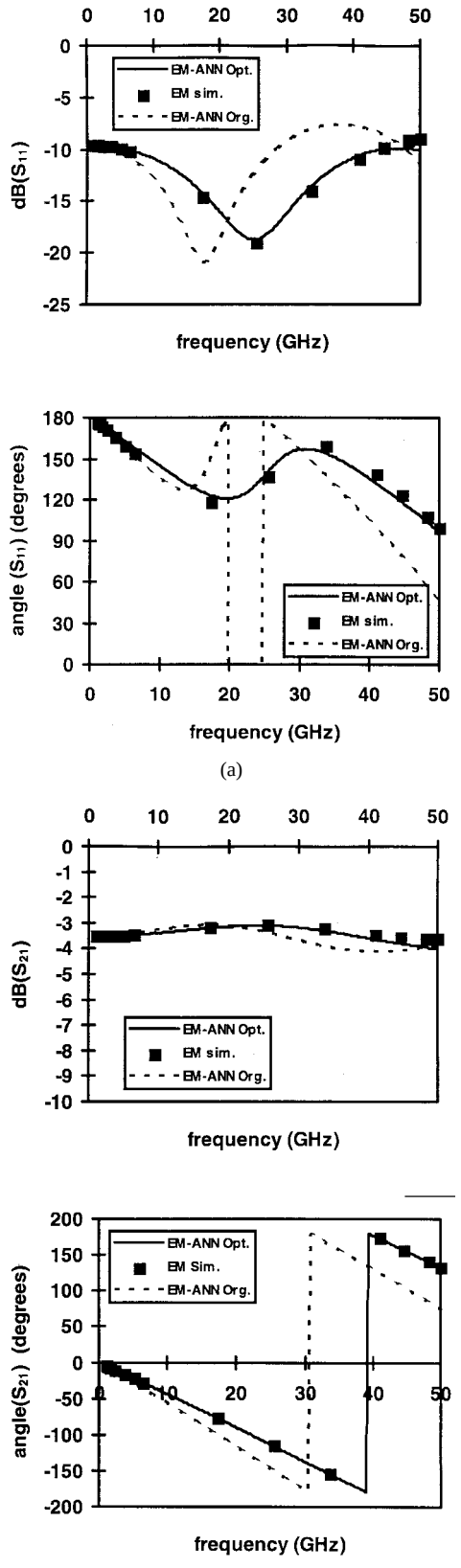

Fig. 14. CPW power-divider response for the optimized EM-ANN circuit (EM-ANN Opt.), the original EM-ANN circuit (EM-ANN Org.), and EM simulation (EM sim.). (a) S_{11} and (b) S_{21}.

time are achievable by using EM-ANN component models, especially when optimization is desired, requiring numerous circuit solves and when these components are to be used over and over in different circuit designs.

It should be mentioned that even larger and more complex circuits can be designed using the developed EM-ANN models. EM simulation of large complex circuits is limited by the computer resources available, and in many cases is not practical. With EM-ANN component modeling, these difficulties are overcome.

IX. Concluding Remarks

Results presented in this paper clearly demonstrate the application of the EM-ANN modeling approach for developing efficient and accurate models for various CPW components and discontinuities. Models developed for CPW lines, open-ends, shorts, steps-in-width, bends, and T-junctions can be conveniently used for efficient and accurate design of various kinds of CPW circuits. The two examples of circuit design and optimization reported in this paper and verification of final design by comparing with EM simulation results validate the modeling and design approach developed.

The methodology of EM-ANN modeling is applicable to other classes of microwave and millimeter-wave circuits (like multilayer circuits, integrated circuit-antenna modules, etc.) for which accurate component models are not available as yet. Thus, we can look forward to increasing applications of the EM-ANN modeling approach in the microwave- and millimeter-wave-design area.

References

[1] M. Wu *et al.*, "Full-wave characterization of the mode conversion in a CPW right-angled bend," *IEEE Trans. Microwave Theory Tech.*, vol. 43, pp. 2532–2538, Nov. 1995.

[2] T. Becks and I. Wolff, "Full-wave analysis of various CPW bends and T-junctions with respect to different types of air-bridges," in *IEEE MTT-S Int. Microwave Symp. Dig.*, Atlanta, Ga, June 1993, pp. 697–700.

[3] A. A. Omar *et al.*, "Effects of air-bridges and mitering on CPW 90° bends: Theory and experiment," in *IEEE MTT-S Int. Microwave Symp. Dig.*, Atlanta, Ga, June 1993, pp. 823–826.

[4] C. Sinclair *et al.*, "Closed-form expressions for CPW discontinuities," in *Conf. Proc. Military Microwaves '92*, Brighton, U.K., Oct. 1992, pp. 227–229.

[5] S. Alexandrou *et al.*, "Time-domain characterization of bent CPW's," *IEEE J. Quantum Electron.*, vol. 28, pp. 2325–2332, Oct. 1992.

[6] R. Bromme and R. H. Jansen, "Systematic investigation of CPW MIC/MMIC structures using a unified strip/slot 3D EM simulator," in *IEEE MTT-S Int. Microwave Symp. Dig.*, Boston, MA, June 1991, pp. 1081–1084.

[7] H. Sawasa *et al.*, "Transmission characteristics of CPW bends for various curvatures," *IEICE Tran. Electron.*, vol. E77-C, pp. 949–951, June 1994.

[8] ——, "Radiation from bend in CPW angular and circular bends," in *Int. Symp. EM Comp.*, Jendai, Japan, May 1994, p. 325.

[9] D. Mirshekar-Syahkal, "Computation of equivalent circuits of CPW discontinuities using quasi-static spectral domain method," *IEEE Trans. Microwave Theory Tech.*, vol. 44, pp. 979–984, June 1996.

[10] M. Nadarassin *et al.*, "Analysis of planar structures by an integral approach using entire domain trial functions," *IEEE Trans. Microwave Theory Tech.*, vol. 43, pp. 2492–2495, Oct. 1995.

[11] F. Mernyei *et al.*, "New cross-T junction for CPW stub-filters on MMIC's," *IEEE Microwave Guided Wave Lett.*, vol. 5, pp. 139–141, May 1995.

[12] M. Naghed *et al.*, "A new method for the calculation of the equivalent inductances of coplanar waveguide discontinuities," in *IEEE MTT-S Int. Microwave Symp. Dig.*, Boston, MA, June 1991, pp. 747–750.

[13] A. Omar *et al.*, "A versatile moment method solution of the conventional and modified coplanar waveguide T-junctions," *IEEE Trans. Microwave Theory Tech.*, vol. 41, pp. 687–692, Apr. 1993.

[14] R. Simons *et al.,* "Modeling of some coplanar waveguide discontinuities," *IEEE Trans. Microwave Theory Tech.,* vol. 36, pp. 1796–1803, Dec. 1988.
[15] M. Naghed *et al.,* "Equivalent capacitances of coplanar waveguide discontinuities and interdigitated capacitors using a three-dimensional finite difference method," *IEEE Trans. Microwave Theory Tech.,* vol. 38, pp. 1808–1815, Dec. 1990.
[16] M. Drissi *et al.,* "Analysis of coplanar waveguide radiating end effects using the integral equation technique," *IEEE Trans. Microwave Theory Tech.,* vol. 39, pp. 112–116, Jan. 1991.
[17] B. Isele and P. Russer, "The modeling of coplanar circuits in a parallel computing environment," in *IEEE MTT-S Int. Microwave Symp. Dig.,* San Francisco, CA, June 1996, pp. 1035–1038.
[18] N. I. Dib *et al.,* "A comprehensive theoretical and experimental study of coplanar waveguide shunt stubs," in *IEEE MTT-S Int. Microwave Symp. Dig.,* Albuquerque, NM, June 1992, pp. 947–950.
[19] M. Yu *et al.,* "Analysis of planar circuit discontinuities using the quasistatic space-spectral domain approach," in *IEEE MTT-S Int. Microwave Symp. Dig.,* Albuquerque, NM, June 1992, pp. 845–848.
[20] R. Doerner *et al.,* "Modeling of passive elements for coplanar SiGe MMIC's," in *IEEE MTT-S Int. Microwave Symp. Dig.,* Orlando, FL, May 1995, pp. 1187–1190.
[21] H. Jin and R. Vahldieck, "Full-wave analysis of coplanar waveguide discontinuities using the frequency domain TLM method," *IEEE Trans. Microwave Theory Tech.,* vol. 41, pp. 1538–1542, Sept. 1993.
[22] M. Yu *et al.,* "Theoretical and experimental characterization of coplanar waveguide discontinuities," *IEEE Trans. Microwave Theory Tech.,* vol. 41, pp. 1638–1640, Sept. 1993.
[23] F. Alessandri *et al.,* "A 3-D matching technique for the efficient analysis of coplanar MMIC discontinuities with finite metallization thickness," *IEEE Trans. Microwave Theory Tech.,* vol. 41, pp. 1625–1629, Sept. 1993.
[24] A. Tran and T. Itoh, "Full-wave modeling of coplanar waveguide discontinuities with finite conductor thickness," *IEEE Trans. Microwave Theory Tech.,* vol. 41, pp. 1611–1615, Sept. 1993.
[25] C. Chiu and R. Wu, "A moment method analysis for coplanar waveguide discontinuity inductances," *IEEE Trans. Microwave Theory Tech.,* vol. 41, pp. 1511–1514, Sept. 1993.
[26] N. I. Dib *et al.,* "Characterization of asymmetric coplanar waveguide discontinuities," *IEEE Trans. Microwave Theory Tech.,* vol. 41, pp. 1549–1557, Sept. 1993.
[27] ———, "A theoretical and experimental study of coplanar waveguide shunt stubs," *IEEE Trans. Microwave Theory Tech.,* vol. 41, pp. 38–44, Jan. 1993.
[28] H. Klingbeil *et al.,* "FDFD full-wave analysis and modeling of dielectric and metallic losses of CPW short circuits," *IEEE Trans. Microwave Theory Tech.,* vol. 44, pp. 485–487, Mar. 1996.
[29] K. Beilenhoff *et al.,* "Open and short circuits in coplanar MMIC's," *IEEE Trans. Microwave Theory Tech.,* vol. 41, pp. 1534–1537, Sept. 1993.
[30] M. Mao *et al.,* "Characterization of coplanar waveguide open end capacitance—Theory and experiment," *IEEE Trans. Microwave Theory Tech.,* vol. 42, pp. 1016–1024, June 1994.
[31] W. Harokopus, Jr. and P. B. Katehi, "Radiation loss from open coplanar waveguide discontinuities," in *IEEE MTT-S Int. Microwave Symp. Dig.,* Boston, MA, June 1991, pp. 743–746.
[32] C. Wguyen *et al.,* "Analysis of coplanar waveguide multiple-step discontinuities," in *IEEE AP-S Symp. Dig.,* Ann Arbor, MI, June 28–July 2, 1993, pp. 185–188.
[33] Y. Lin, "Characterization of coplanar waveguide open-end and short-end discontinuities by the integral equation method," in *Asia–Pacific Microwave Conf. Dig.,* Hsinchu, Taiwan, Oct. 1993, pp. 29–32.
[34] P. Pogatzki *et al.,* "A comprehensive evaluation of quasistatic 3D-FD calculations for more than 14 CPW structures—Lines, discontinuities, and lumped elements," in *IEEE MTT-S Int. Microwave Symp. Dig.,* San Diego, CA, May 1994, pp. 1289–1292.
[35] P. Pogatzki and O. Kramer, "A coplanar element library for the accurate CAD of (M)MIC's," *Microwave Eng. Europe,* pp. 41–46, Dec. 1993/Jan. 1994.
[36] M. Riaziat *et al.,* "Coplanar waveguides used in 2–18 GHz distributed amplifier," in *IEEE MTT-S Int. Microwave Symp. Dig.,* Baltimore, MD, June 1986, pp. 337–338.
[37] P. M. Watson and K. C. Gupta, "EM-ANN models for via interconnects in microstrip circuits," in *IEEE MTT-S Int. Microwave Symp. Dig.,* San Francisco, CA, June 1996, pp. 1819–1822.
[38] ———, "EM-ANN models for microstrip vias and interconnects in multilayer circuits," *IEEE Trans. Microwave Theory Tech.,* vol. 44, pp. 2495–2503, Dec. 1996.
[39] C. M. Bishop, *Neural networks for pattern recognition.* New York: Oxford Univ. Press, 1996.
[40] M. Marwah, Y. Lee, and R. L. Mahajan, "Integrated neural network modeling for electronic manufacturing," *J. Electron. Manufacturing,* vol. 6, no. 2, pp. 79–91, June 1996.
[41] D. C. Montgomery, *Design and Analysis of Experiments.* New York: Wiley, 1991.
[42] P. M. Watson and K. C. Gupta, "EM-ANN modeling and optimal chamfering of 90° CPW bends with air-bridges," in *IEEE MTT-S Int. Microwave Symp. Dig.,* Denver, CO, June 1997, pp. 1603–1606.

Paul M. Watson was born in Ogden, UT, in May 1968. He received the B.S. and M.S. degrees in electrical engineering from the University of Utah, Salt Lake City, in 1991 and 1993, respectively, and is currently working toward the Ph.D. degree in electrical engineering from the University of Colorado at Boulder.

His main research interests are in the area of neural-network modeling of MMIC components for use in interactive CAD.

Kuldip C. Gupta (M'62–SM'74–F'88), for a photograph and biography, see this issue, p. 2173.